Novel Ionising Radiation Detection Systems

Cinzia Da Vià

The University of Manchester, UK & Stony Brook University USA

Radiation Detectors and Imaging Systems are used in many scientific fields. → Several detector requirements seem to be converging with time

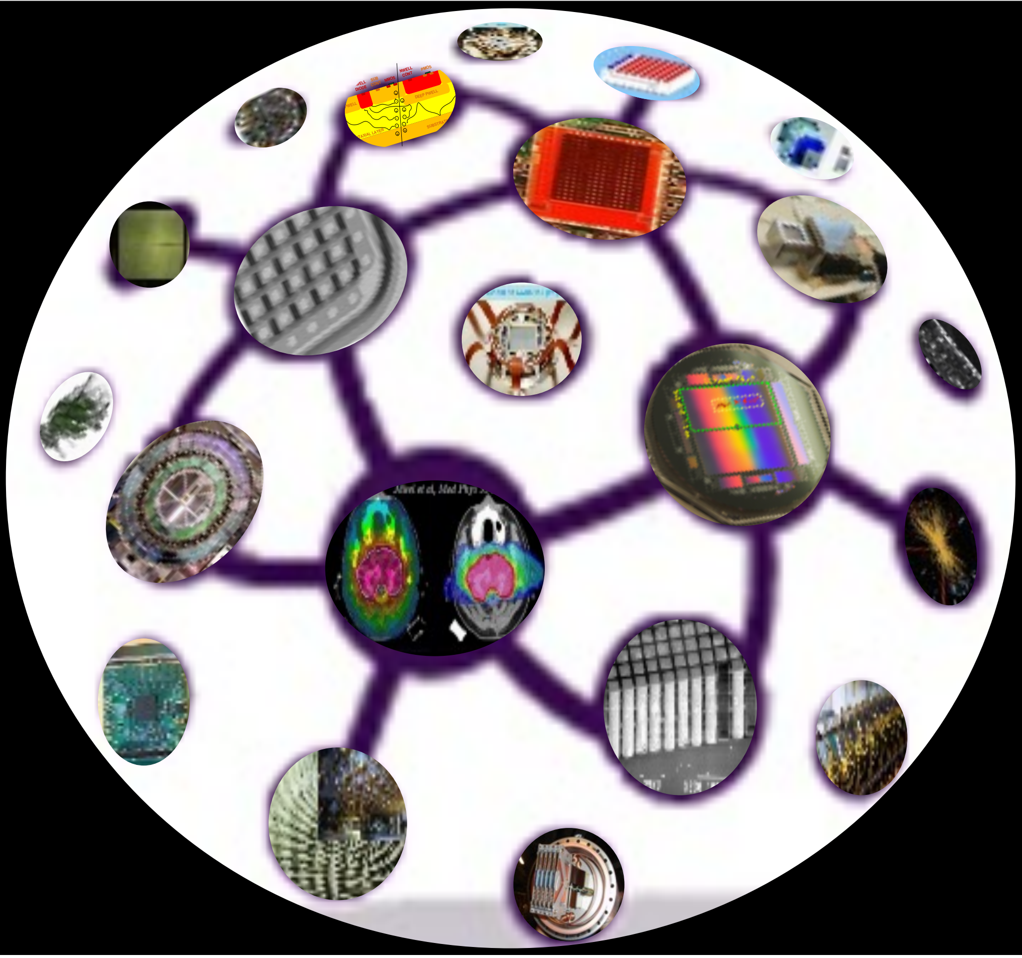

Overviews in this conference:

- **High Energy Physics**
  - *Applications in Particle Physics, P. Riedler, Wednesday, 14:00*
- **Synchrotron Applications**
  - *Detectors for FELS, Synchrotrons and Other Advanced Light Sources H. Grafsma Monday 9:20*
- **Nuclear Physics**
  - *Applications in Nuclear Physics and Nuclear Industry TBC, Tuesday 14:00*
- **Neutron Facilities Sources**
  - *Detectors for Neutron Facilities, R Hall-Wilton Tuesday 16:15*
- **Life Sciences and Biology**
  - *Applications in Life Sciences and Biology, M. Campbell, Thursday 8:40*
- **Medical Imaging**
  - *Medical Applications of Position Sensitive Detectors Reinhard Schulte, Monday 16:15*
- **Astroparticles**
  - *Applications of Astro-particle Physics Position Sensitive Detectors, R. Johnson, Wednesday 16:55*
- **Astronomy, Space Applications**
  - *Applications in Astronomy, Planetary and Space Science A. Holland Tuesday 9:00*
- **Security and Environmental Monitoring**
  - *Applications in Security and Environmental Imaging, V. Schoepff, Friday 8:40*

Collection of Radiation Detectors Requirements “wishes” among Application Fields in 2016

https://indico.cern.ch/event/244890/

	HEP	SYNC	Neutron ESS	Beam monitoring	Astronomy	Hadron Therapy	Medical Imaging Pre-clinical Imaging	Electron Microscopy	Environmental radiation monitoring
Radiation type	p, n, γ	X-rays	n	p, n, γ, e^-	λ=300nm to 28µm	N, p, γ, light ions (protons to oxygen)	X-rays	e	γ
Max Intensity	12x10 ^{15} ncm^{-2}	2700 pulses	10 ^{8} ncm^{-2}	10 ^{17} ncm^{-2} (p, n) 10MGy (e^-)	from 1 photon/hour/pixel to 1E9 photons/s/pixel	conventional accelerator up to 10^10 ions /s Laser > 10^7/cm2 (ps pulses, low repetition rate ~ 1/s)	CT: 10^{9} g/mm^{2}/s, General X-ray: 10^{8} g/mm^{2}/s Angiography: 10^{8} g/mm^{2}/s Mammography: 10^{7} g/mm^{2}/s	20 Mrads	100 µSv/h (~100,000 cts/s)
timing	25ns 10ps	4.5 MHz	1us	Sub ns	from 2000 frames/s to 1 frame/hour	Up to MHz (singles rate)	CT: 5000 frames/s General X-ray: - Angiography: 1-60 frames/s Mammography: -	1000 frames/s	--
Pixel size (Min)	50x50 um^{2}	10x10um^{2}	50x50 um^{2}	50x50 um^{2}	10µmx10µm	50 um	CT: 1000 um General X-ray: 150-200 um Angiography: 150-200 um Mammography: 85 um	10x10um^{2}	--
Spectral resolution	yes	yes	no	yes	no , moderate possible with APD	yes	Today: not used, Future: yes	yes	< 1.5% @ 662 keV
Detector size (max)	2500m^{2} (ILC cal)		80m^{2}	100 cm^{2}	Optical 9Kx9K NIR 4Kx4K	40x40 cm2	CT: 10 x 100 cm^{2} (segmented), General X-ray : 43x43 cm^{2} Angiography: 30x40 cm^{2} Mammography: 24x30 cm^{2}	8k x 8k pixels	6 cm^{3}

Cinzia Da Via, Stony Brook USA and The University of Manchester, UK– 2021

Novel Detector Systems Common Trends

Space
Time
Energy

precision

Materials
Electronics
Interconnection

large area

Mix & Match

2D materials
3D printing
2D Integration

Micro-fabrication
Meta-Nano materials
AI-Quantum I

Emerging
Technology
trends

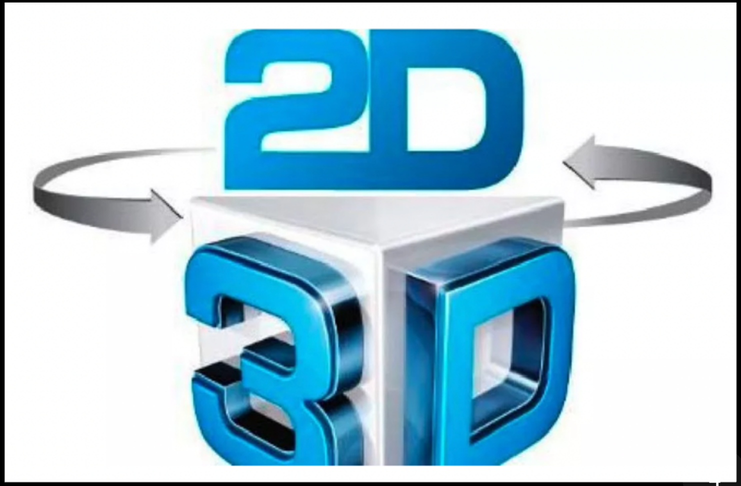

2D materials

Sensors (Basel). 2016 Feb; 16(2): 223.

Graphene
2004 isolated
2010 Nobel

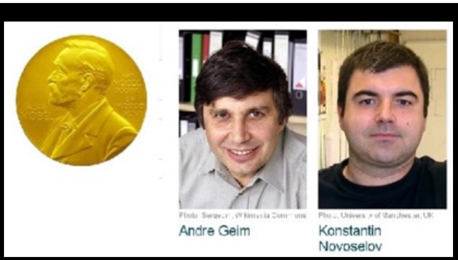
Andre Geim
Konstantin Novoselov

“2D materials Beyond Graphene”

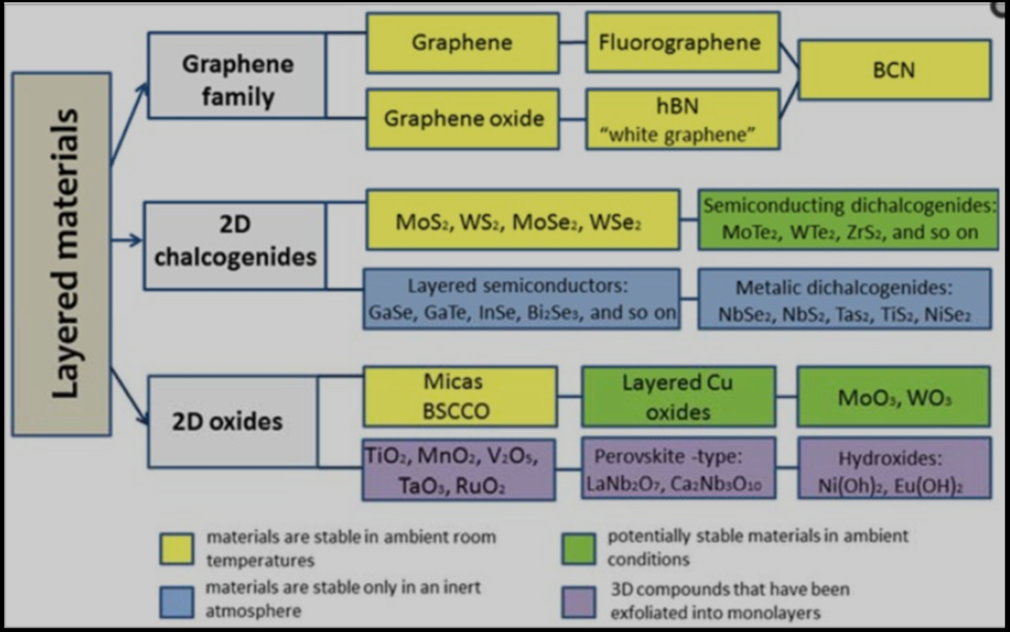

hexagonal boron nitride

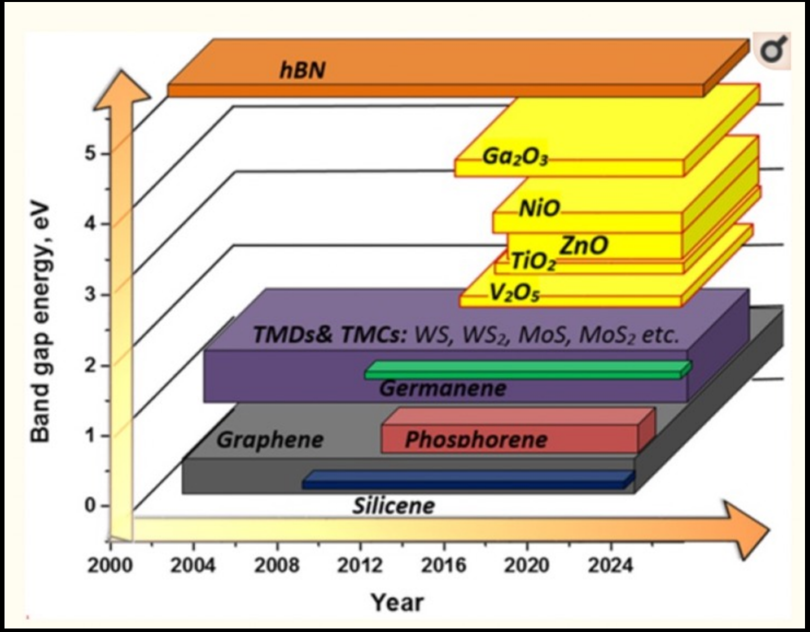

3D layers of 2D materials semiconductors

- *192 | NATURE | VOL 490 | 11 OCTOBER 2012*
- *Z. Fang et al. ISSN 1998-0124 CN 11-5974/04 2018*

Strategies of 2D materials-based assembly into integrated functional nanostructures

Example in optoelectronics:

Two graphene layers are separated by several layers of boron-nitride, which serve as a tunneling barrier.

A built-in electric field (created by the proximity of one of the graphene layers to a monolayer of MoS_2 molybdenum di-sulfite) separates the electron–hole pair, which is created by an incoming particle.

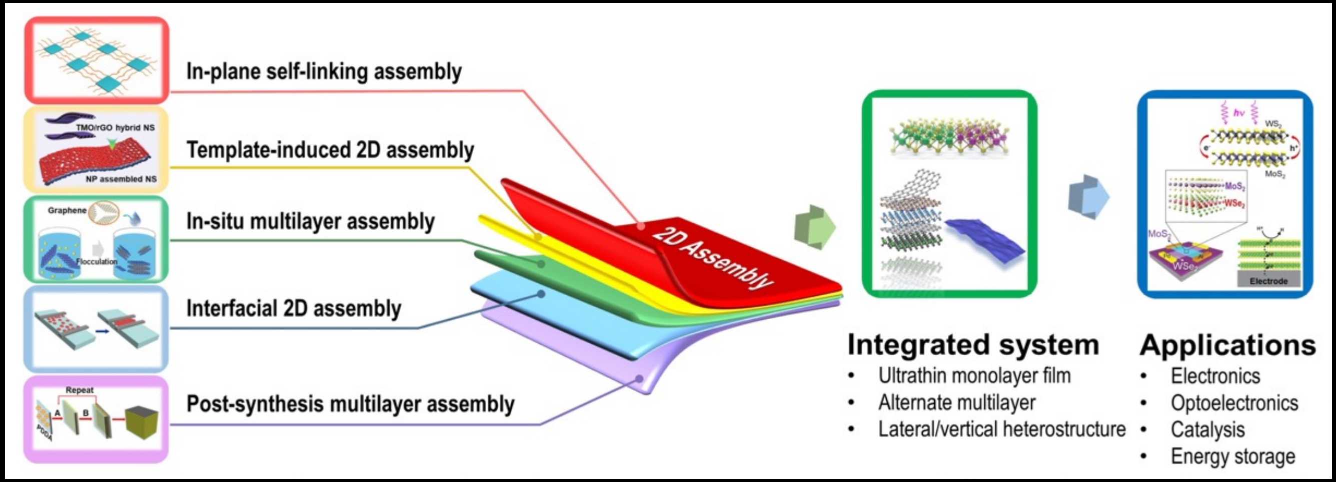

Integrated system
- Ultrathin monolayer film
- Alternate multilayer
- Lateral/vertical heterostructure

Applications
- Electronics
- Optoelectronics
- Catalysis
- Energy storage

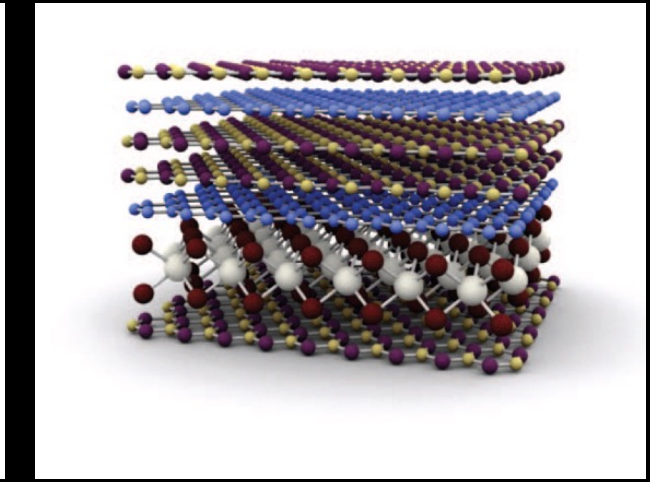

Latest news on graphene semiconductors

https://www.graphene-info.com/news

The European Commission announces a €20 million investment in a new plant for graphene electronics

The European Commission (EC) has announced a €20 million investment in the next generation of electronics and semiconductors. The 2D Experimental Pilot Line (2D-EPL) was officially launched as the first graphene foundry to integrate graphene and layered materials into semiconductor platforms. The new project aims to keep Europe at the forefront of this technological revolution.

Researchers manage to grow GNRs directly on top of silicon wafers

Scientist from the University of Wisconsin-Madison are working towards making more powerful computers a reality. To that end, they have devised a method to grow tiny ribbons of graphene directly on top of silicon wafers. Graphene ribbons have a special advantage over graphene sheets - they become excellent semiconductors.

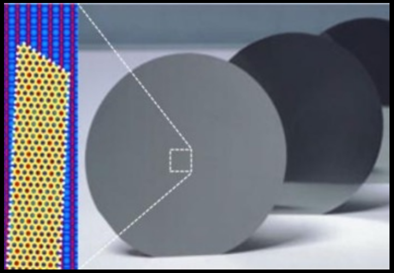

Researchers bind hydrogen to graphene in a super-fast reaction that also opens up a bandgap

Researchers from Göttingen and Pasadena (USA) have produced an "atomic scale movie" showing how hydrogen atoms chemically bind to graphene in one of the fastest reactions ever studied. The team found that by adhering hydrogen atoms to graphene, a bandgap can be formed.

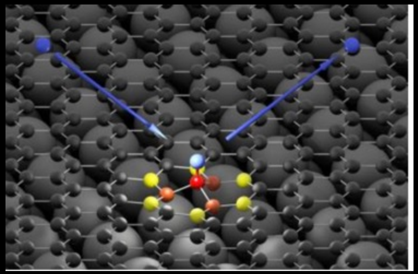

Team creates artificial graphene in a semiconductor structure

Researchers at Columbia Engineering, working with colleagues from Princeton and Purdue Universities and Istituto Italiano di Tecnologia, have engineered "artificial graphene" by recreating, for the first time, the electronic structure of graphene in a semiconductor device.

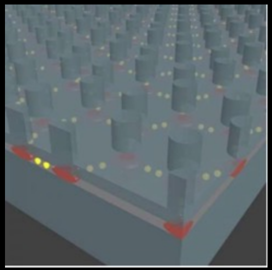

MIT team uses graphene as a "copy machine" for semiconductors

Researchers at MIT have developed a technique that uses graphene as a kind of “copy machine”, to transfer intricate crystalline patterns from an underlying semiconductor wafer to a top layer of identical material.

Graphene radiation detectors

M. Foxe et al. IEEE Trans. Nanotech. 11, 581 (2012)

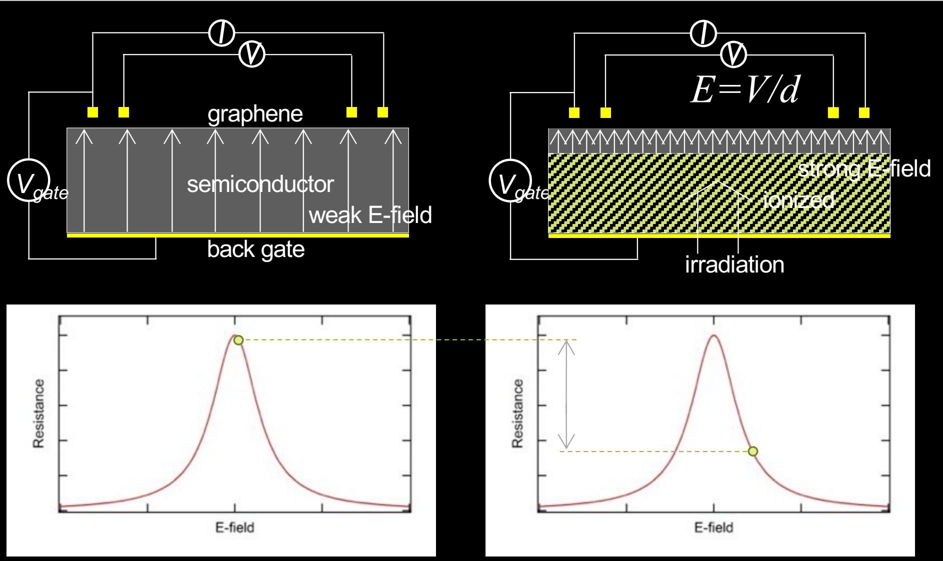

Graphene exhibits a sharp change in resistance as a function of applied field, near the charge neutrality point ("Dirac point")

- NOT relying on collecting ionized charges but on the change of electric field produced by them
- Can work with variety of absorber substrates best suited: gamma/neutron interaction; room-T (wide bandgap); energy resolution (narrow bandgap) - less stringent requirement on substrate mobility etc.
- Low noise (even at room T), Graphene (semimetal) resistance stays finite

Response to X rays

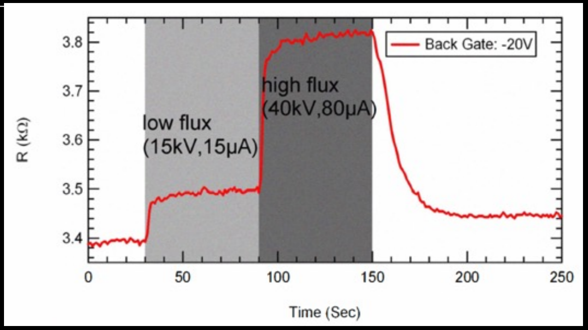

Silicon substrate

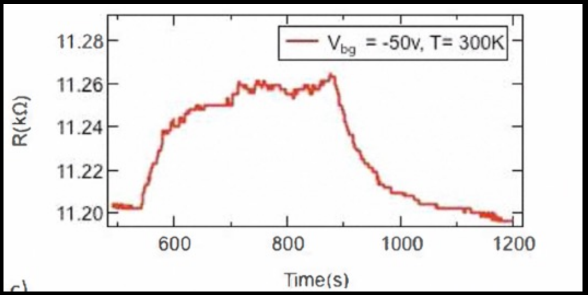

SiC substrate

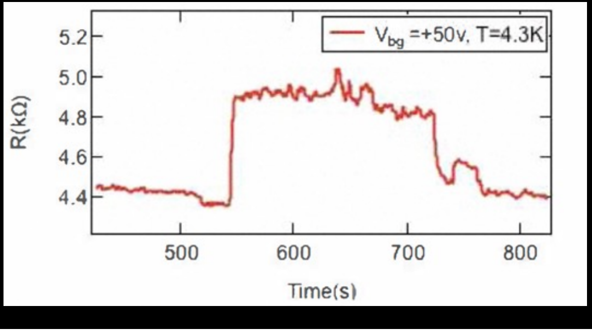

GaAs substrate

Intrinsic response time of Graphene Photodetectors

A. Urich et al. Nano Lett. 2011, 11, 2804-2808

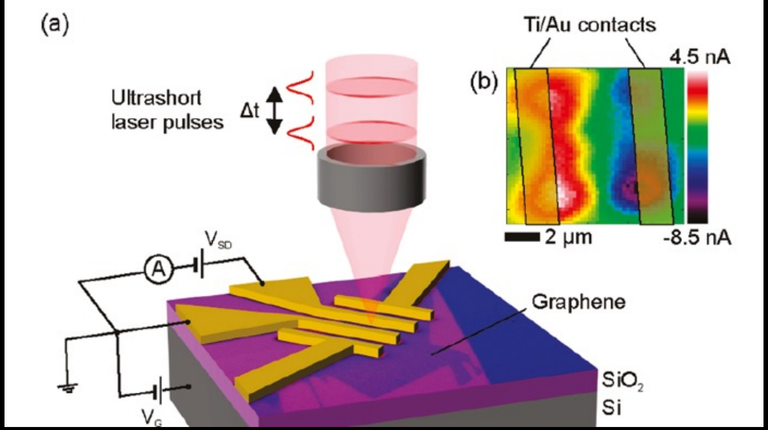

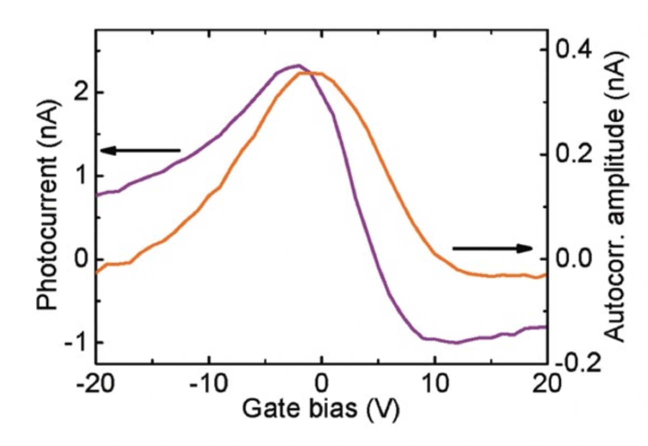

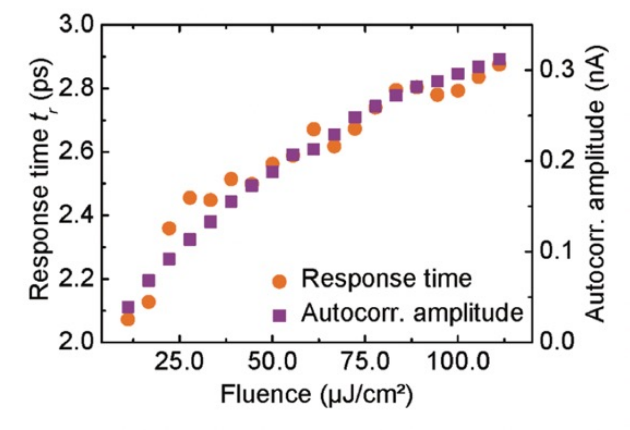

- Graphene on SiO_2 (20nm) and Si
- 2 laser beams 100fs pulse length
- 1.55um wavelength
- Second order interference mechanism
- Intrinsic response time of generated photocurrent ~2.1ps

Graphene Oxide films for field effect surface silicon passivation

M. Vaqueiro-Contreras et al.
Solar Energy Materials and Solar Cells 187 (2018) 189-193

Used in Schottky barrier solar cells – enhanced efficiency possibly due to dangling bonds saturation at the surface

Minority lifetimes maps of a double polished FZ p-type 1 kohm-cm Silicon sample without (a) and with (b) GO coating

Silicon Thickness from 200-625 um

GO thickness = 200 nm

Single polished sample CZ p-type 2.8 ohm-cm Si without (c) and with (d) GO coating

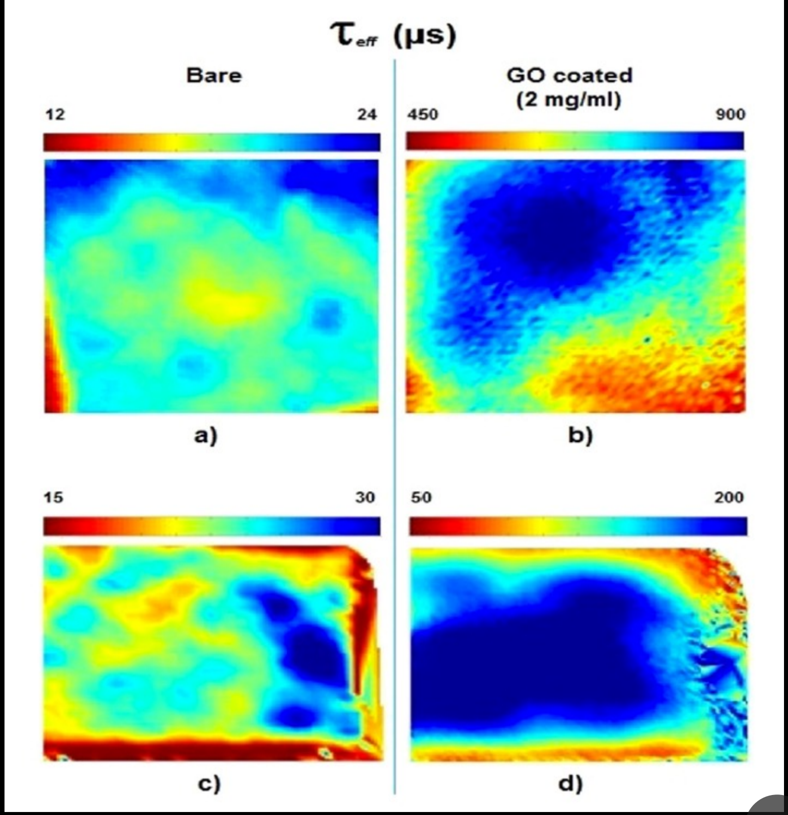

3D printing is commercially here to stay

XXL additive manufacturing:

https://all3dp.com/1/3d-printed-house-homes-buildings-3d-printing-construction/

https://www.sculpteo.com/en/materials/

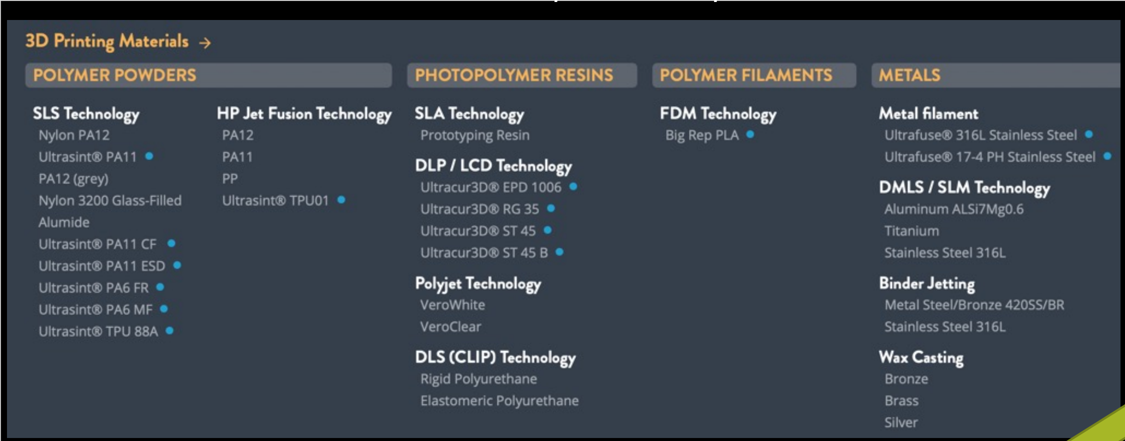

3D Printing Materials →

POLYMER POWDERS

SLS Technology
- Nylon PA12
- Ultrasint® PA11 ●
- PA12 (grey)
- Nylon 3200 Glass-Filled
- Alumide
- Ultrasint® PA11 CF ●
- Ultrasint® PA11 ESD ●
- Ultrasint® PA6 FR ●
- Ultrasint® PA6 MF ●
- Ultrasint® TPU 88A ●

HP Jet Fusion Technology
- PA12
- PA11
- PP
- Ultrasint® TPU01 ●

PHOTOPOLYMER RESINS

SLA Technology
- Prototyping Resin

DLP / LCD Technology
- Ultracur3D® EPD 1006 ●
- Ultracur3D® RG 35 ●
- Ultracur3D® ST 45 ●
- Ultracur3D® ST 45 B ●

Polyjet Technology
- VeroWhite
- VeroClear

DLS (CLIP) Technology
- Rigid Polyurethane
- Elastomeric Polyurethane

POLYMER FILAMENTS

FDM Technology
- Big Rep PLA ●

METALS

Metal filament
- Ultrafuse® 316L Stainless Steel ●
- Ultrafuse® 17-4 PH Stainless Steel ●

DMLS / SLM Technology
- Aluminum ALSi7Mg0.6
- Titanium
- Stainless Steel 316L

Binder Jetting
- Metal Steel/Bronze 420SS/BR
- Stainless Steel 316L

Wax Casting
- Bronze
- Brass
- Silver

2 story villa
- Concrete
- 20 tons
- 45 days

2016 Guinness World Records title

Boeing 777x wing

- 5.3m long, 1.7 m wide and 0.5 m tall
- 30 hours (rather than 3 months)
- 748kg

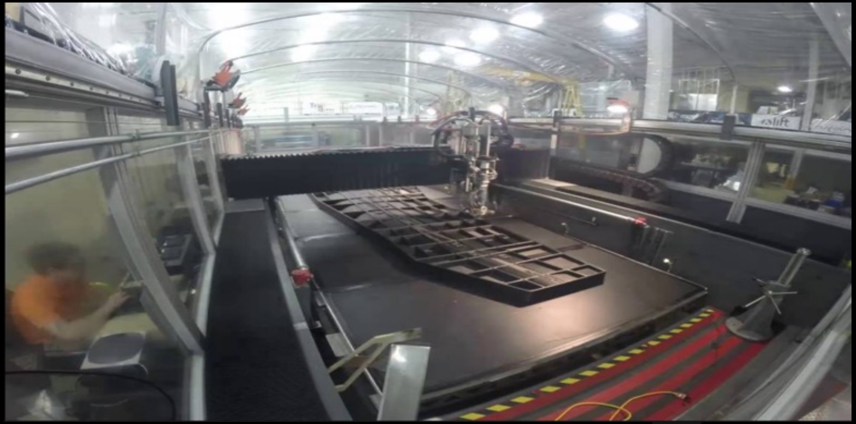

Oak Ridge National Laboratory

ACS Nano 2021, 15, 4077–4084

3D printing perovskites onto graphene creates ultrasensitive X-ray detector

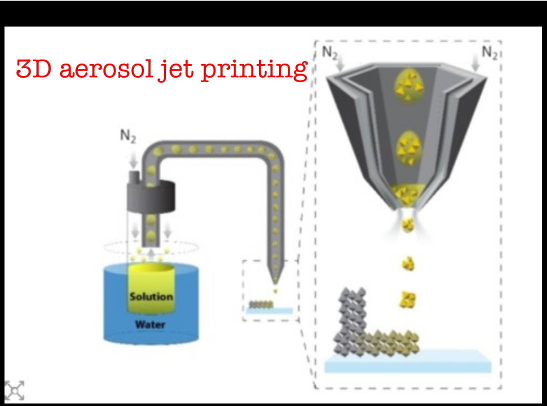
3D aerosol jet printing

perovskite methylammonium lead iodide (MAPbI$_3$) on graphene

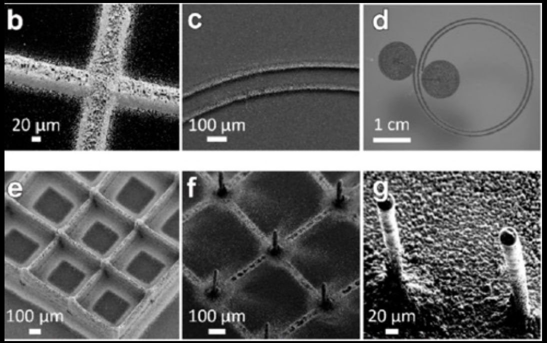

Various printed patterns of MAPbI3 lines, spirals, grids, and pillars written on the glass substrate

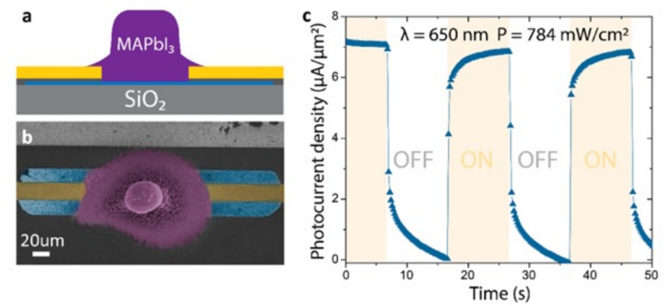

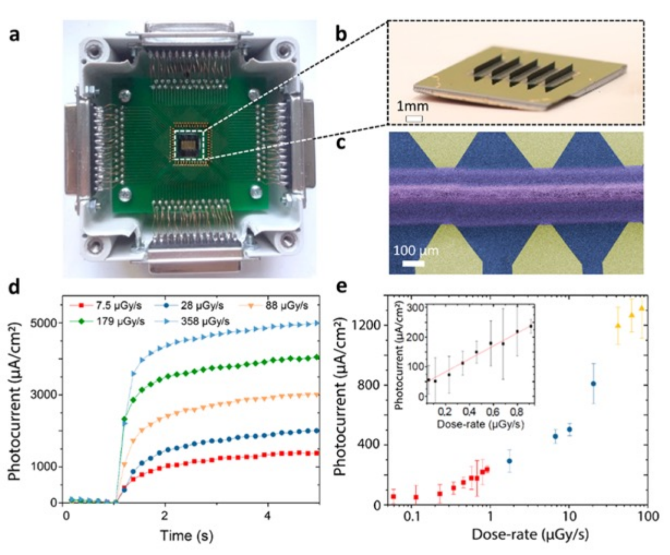

2.2 × 10^{8}µC/Gy$_{air}$/cm^2 when detecting 8 keV X-ray photons at low dose rates

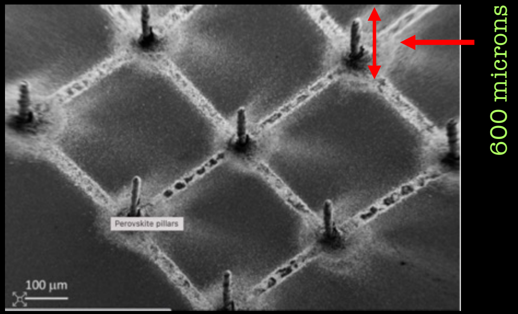

X-ray detector measurements.

(a) Photograph of the fully integrated X-ray detector;
(b) 1 cm^2 sensing chip with 3D-printed MAPbI3 walls about 600 µm in height;
(c) false-colored SEM image of the 3D-printed MAPbI3 wall on the Ti/Au electrodes (graphene in blue, MAPbI3 in purple, and metal electrodes in yellow);
(d) X- ray illumination-induced photocurrent response as a function of time at 100 mV bias voltage;
(e) photocurrent density as a function of X-ray dose rate; region below 1 µGy/s is in the inset.

Cinzia Da Via, Stony Brook USA and The University of Manchester, UK– 2021

3D printed silicon

Adv. Funct. Mater. ***2012****, 22, 4004-4008*

→Objective: micro-nano structures in silicon without the need of a cleanroom

- The layer-by-layer fabrication is based on alternating steps of chemical vapor deposition of silicon and local implantation of gallium ions by focused ion beam (FIB) writing.
- In a final step, the defined 3D structures are formed by etching the silicon in potassium hydroxide (KOH), in which the local ion implantation provides the etching selectivity.
- The method is demonstrated by fabricating 3D structures made of two and three silicon layers, including suspended beams that are 40 nm thick, 500 nm wide, and 4µm long, and patterned lines that are 33 nm wide.

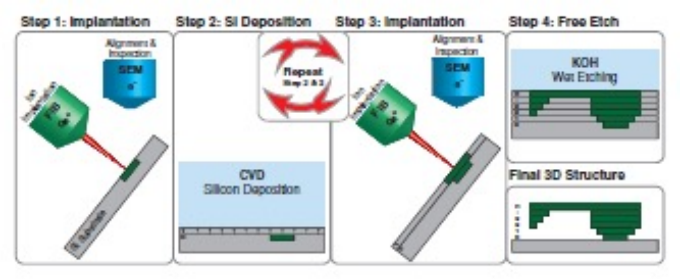

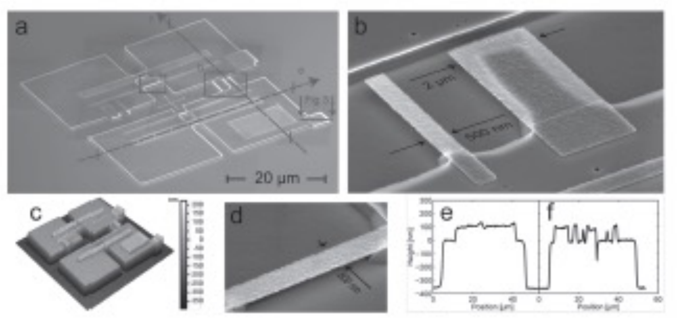

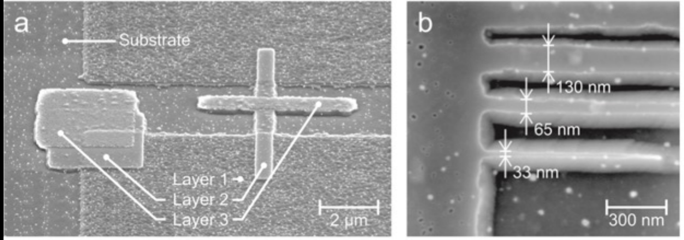

Figure 6. a) An SEM image of 3-layer structures. b) An SEM image of lines of widths as small as 33 nm, patterned in a deposited layer.

G. A. Dosovitskiy et al., CrystEngComm, 2017, 19, 4260-4264

3D-printed complex inorganic polycrystalline scintillator YAG:Ce

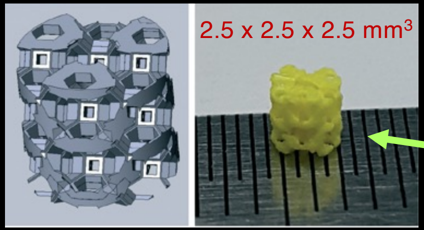

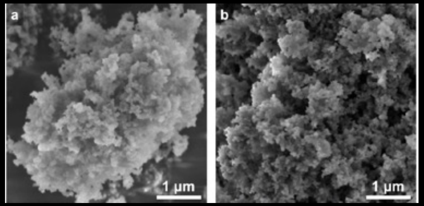

SEM images of YAG-Ce a) dried precipitate and b) powder after calcination at 900 °C.

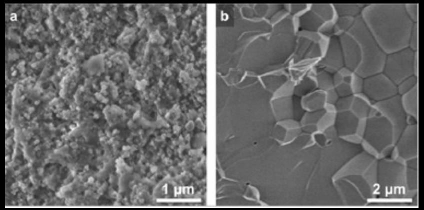

SEM images of a) printed green body (scale) and b) sintered body (left side – scale, right side – free surface).

YAG:Ce (Yttrium Aluminum Garnet doped with Cerium) scintillating material

A green body was printed using a stereophotolithography approach from co-precipitated powders and then sintered at 1600 °C in air to afford translucent ceramics.

The scintillation light yield using 5.5 MeV α-particle excitation was more than 60% higher than that of the reference YAG:Ce single crystal.

High scintillation light yield due **to high activator (Ce) concentration** This is impossible in monocrystalline YAG-Ce which is **0.1-0.5%**

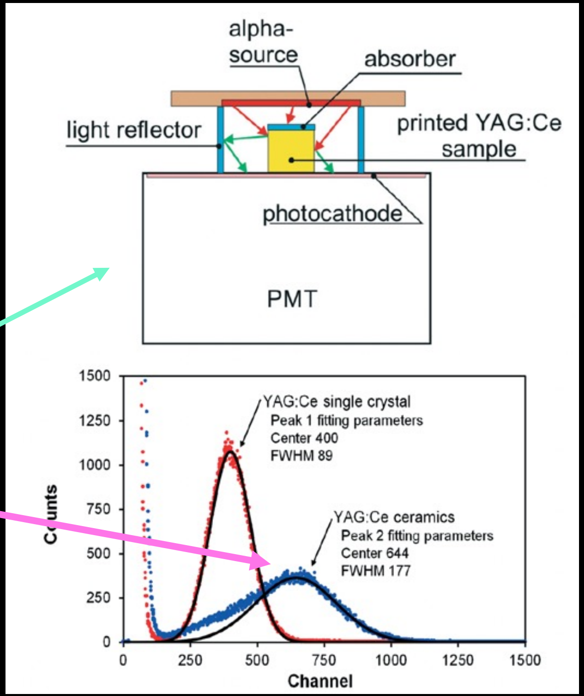

Scintillation pulse height spectra of YAG:Ce printed ceramic sample and reference single crystal under 5.5 MeV α-particles measured in “reflection” geometry

Performance of 3D printed plastic scintillators for gamma-ray detection (477keV)

D. Kim et al. Nuclear Engineering and Technology 52 (2020) 2910-2917

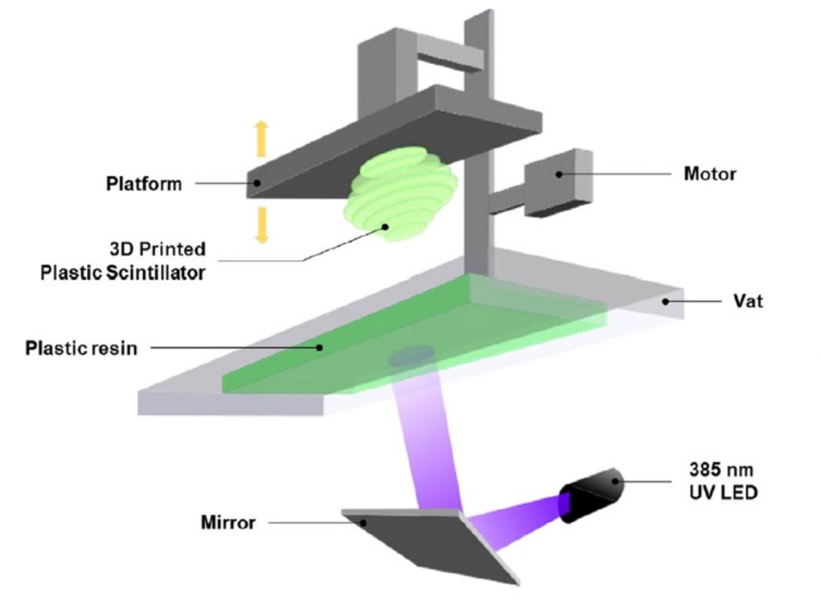

- Digital Light Processing Technology
- UV-LED curing machine
- 67% light output relative to that of BC408,
- Transmittance of 74% relative to that of BC408

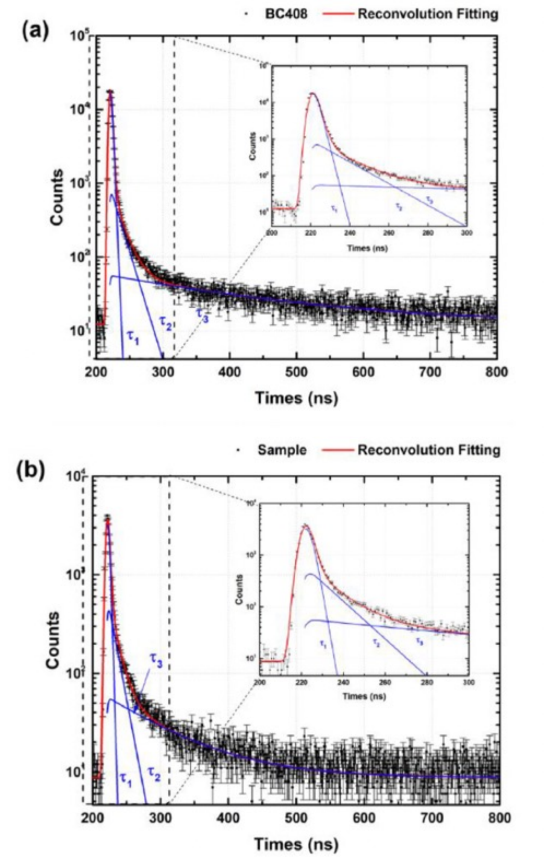

- Average decay time constants of 15.6 ns
- Intrinsic energy resolution of 13.2%for 477 keV
- Intrinsic detection efficiency of 6.81% for 477 keV
- Compton electrons from the ^{137}Cs gamma-ray source.

3D-Printed quantum dots - QLEDs

Nano Lett., **2014**, *14* (12), pp 7017–7023

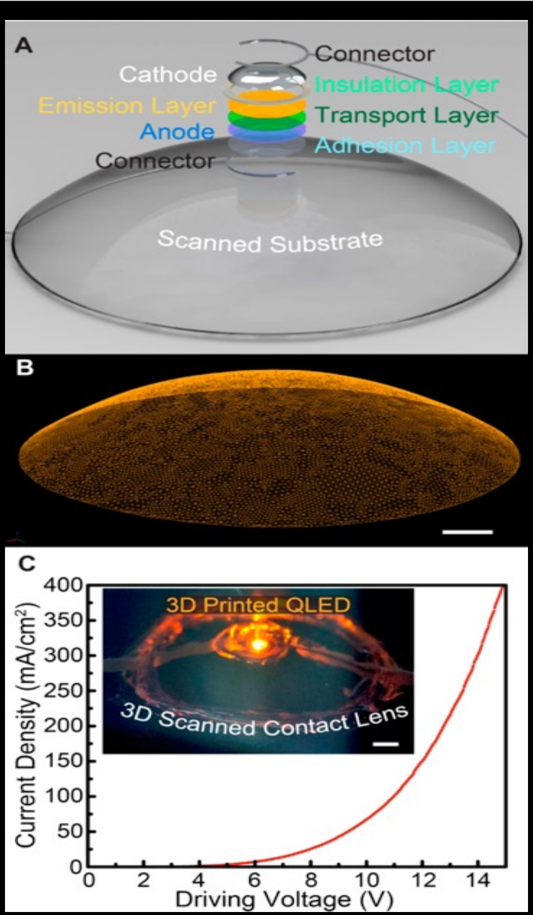

3D printed 2×2×2 multidimensional array of embedded QD-LEDs.

Layout of the multi-color 3D QD-LED array design

3D printed quantum dot light-emitting diode (QLED) on a 3D scanned curvilinear substrate.

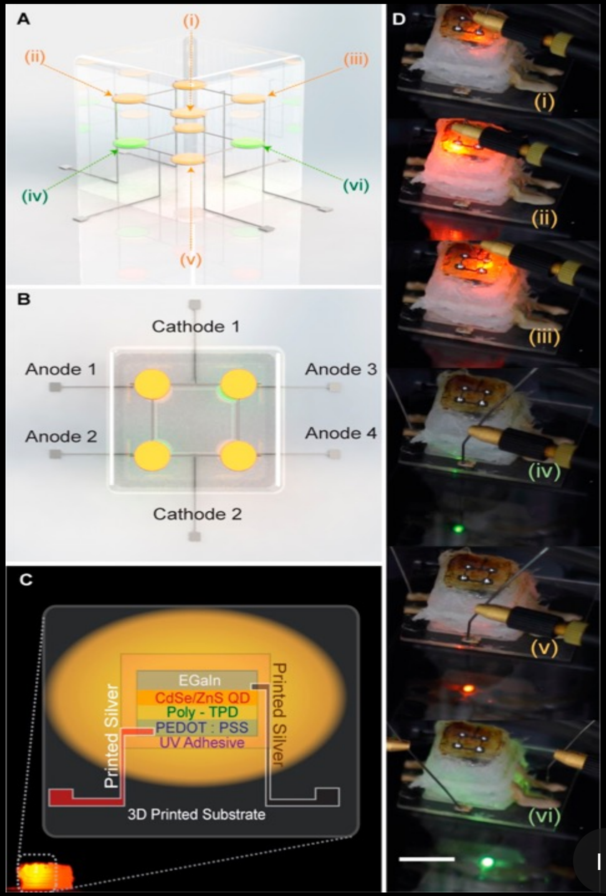

Metamaterials

Combination of in repeating patterns of plastic, metal, etc at **scales that are smaller than the wavelengths of the phenomena they influence**

Metasurfaces are mainly divided into resonance and waveguide types, but can be further classified into several classes depending on their operation wavelengths and application design. Resonance metasurfaces are classified into plasmonic and Mie resonance-based all-dielectric types.

Their precise shape, geometry, size, orientation and arrangement give them their smart properties capable of manipulating electromagnetic waves by blocking, absorbing, enhancing, or bending waves, to achieve benefits that go beyond what is possible with conventional materials.

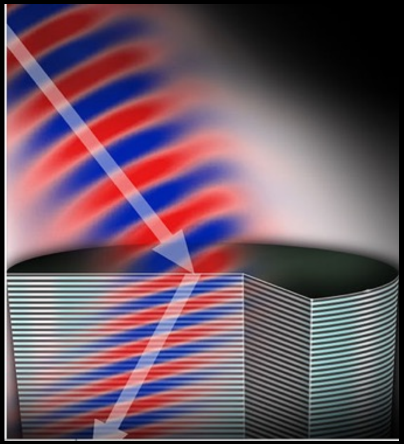

Negative refractive index

1. Lin, D. M. et al, Dielectric Gradient Metasurface Optical Elements. Science 2014, 345 (6194), 298–302.
2. Yu, N.; Capasso, F. Flat Optics with Designer Metasurfaces. Nat. Mater. 2014, 13 (2), 139–150.
3. Kamali, S. et al A Review of Dielectric Optical Metasurfaces for Wavefront Control. Nanophotonics 2018, 7 (6), 1041–1068.
4. Ding, F. et al, Gradient Metasurfaces: A Review of Fundamentals and Applications. Rep. Prog. Phys. 2018, 81 (2), 026401.
5. Li, X.; et al,Multicolor 3D Meta-Holography byBroadband Plasmonic Modulation. Sci. Adv. 2016, 2 (11), e1601102.
6. Zhang, Q. et al, Design of Beam Deflector, Splitters, Wave Plates and Metalens Using Photonic Elements withDielectric Metasurface. Opt. Commun. 2018, 411, 93–100.
7. Chen, W. T.et al, . A Broadband Achromatic Metalens for Focusing and Imaging in the Visible. Nat. Nanotechnol. 2018, 13 (3),220–226.
8. Khorasaninejad, M.et al, Achromatic Metalens Over 60 nm Bandwidth in the Visible and Metalens with Reverse Chromatic Dispersion. Nano Lett. 2017, 17 (3), 1819–1824.
9. Sun, I. K. et al,Dual-Ended Readout of Bismuth Germanate to Improve Timing Resolution in Time-Of-Flight PET. Phys. Med. Biol. 2019, 64,105007
10. Villalpando, A. I et al, Improving the Light Collection Efficiency of Silicon Photomultipliers through the Use of Metalenses.J. Instrum. 2020, 15 (11), P11021.
11. Nemallapudi, M. V et al, Single Photon Time Resolution of State of the Art SiPMs. J. Instrum. 2016, 11 (10), P10016.
12. Lecoq, P. Pushing the Limits in Time-Of-Flight PET Imaging. I.E.E.E. Trans. Radiat. Plasma Med. Sci. 2017, 1 (6), 473–485.
13. Mikheeva, E. et al, CMOS-Compatible All- Dielectric Metalens for Improving Pixel Photodetector Arrays.A.P.L. Photon. 2020, 5 (11), 116105

40 x 40 Metalens Array for Improved Hamamatzu Silicon Photomultiplier Performance

Soh Uenoyama and Ryosuke Ota ACS Photonics 2021, 8, 1548–1555*

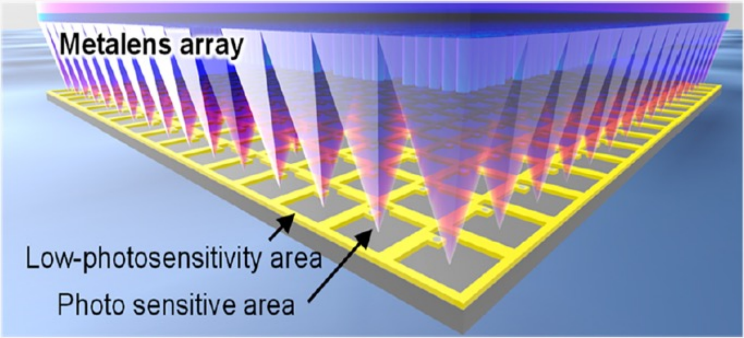

3x3mm^2
75um

~82%
Fill factor

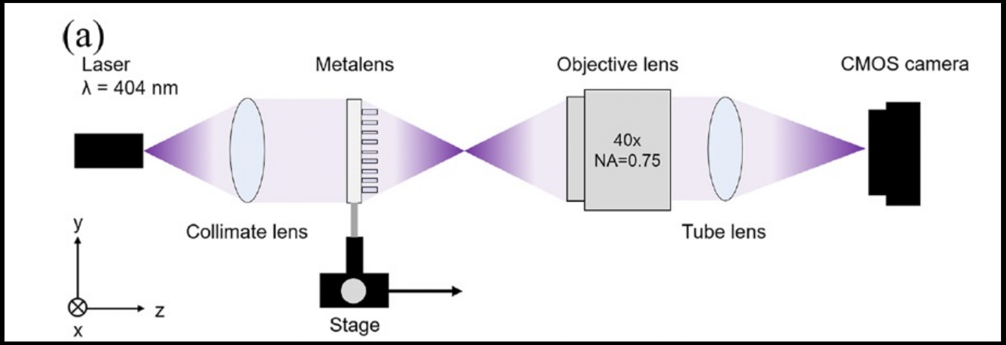

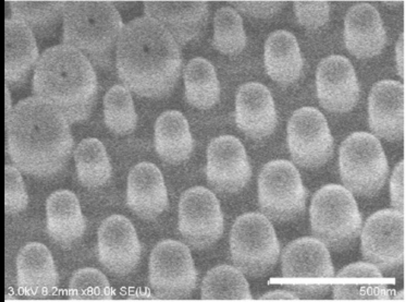

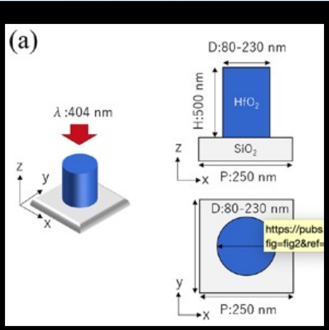

Hafnium oxide (HfO2) nanopillars on a 300 μm thick glass substrate to minimise absorption in the Near UV

Focal Point →
~14.5um
Outside
focal point

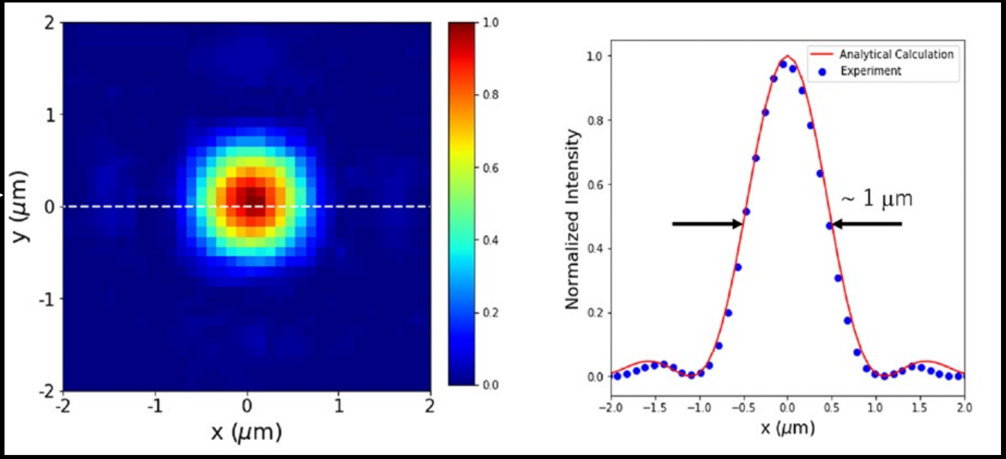

circular transmission nanopillar varies the locally effective index by changing the diameter of the metasurface and does not depend on incident polarization.

40 x 40 Metalens 3x3mm Array for Improved Hamamatzu Silicon Photomultiplier Performance

Soh Uenoyama and Ryosuke Ota ACS Photonics 2021, 8, 1548–1555*

Detection Efficiency improved by ~10% , time resolution by ~6% depending on position

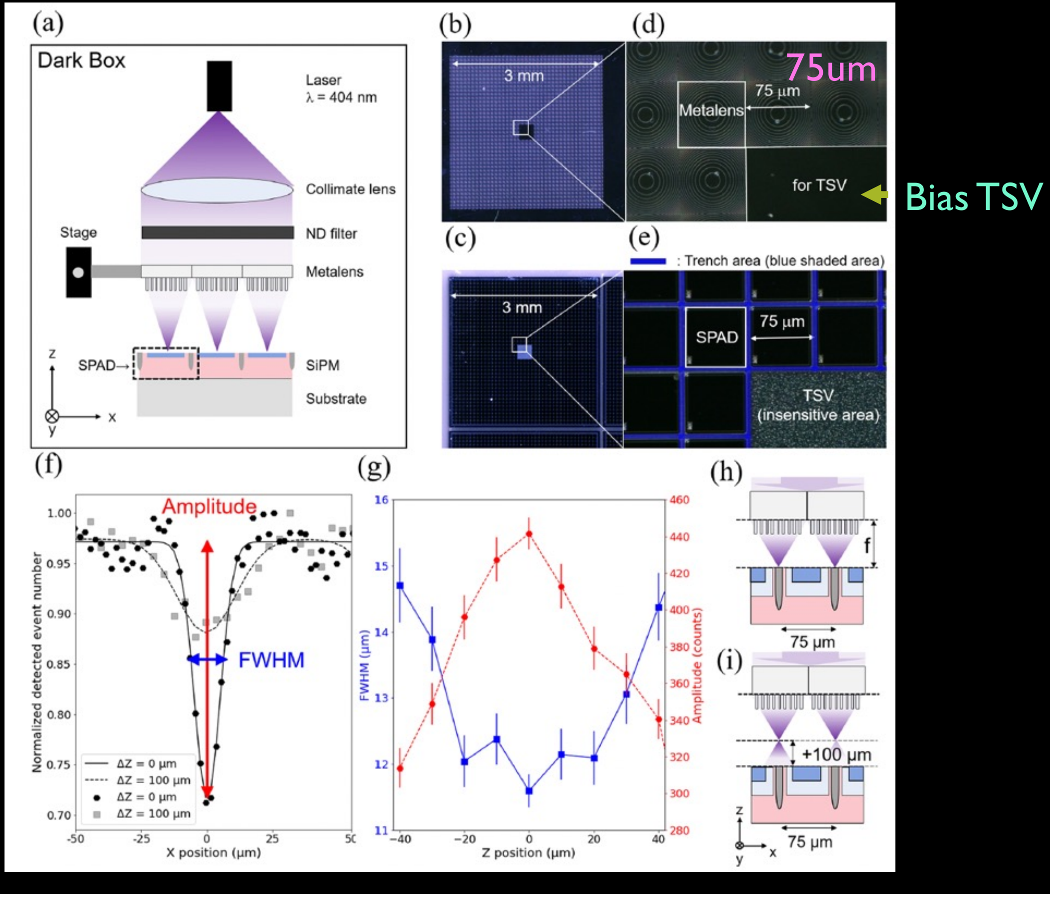

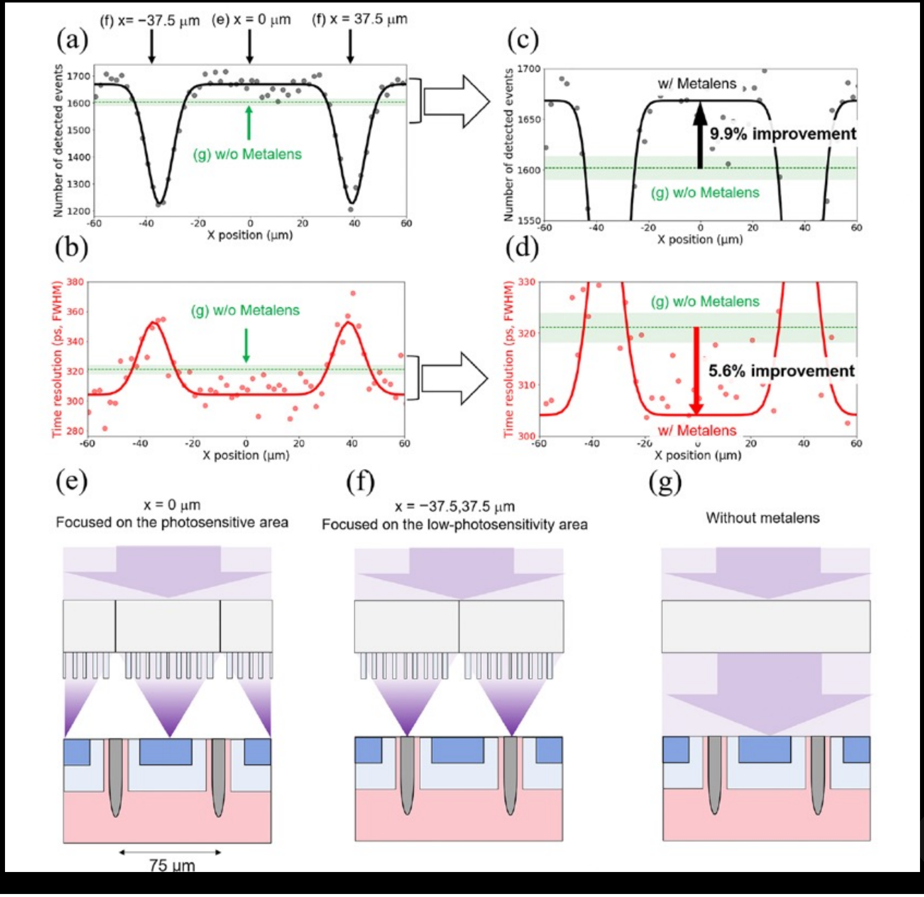

Silicon-Interconnect Fabric

inspired by Gene Amdahl’s wafer-scale integration concept of the late 1980s

IEEE Spectrum *PUNEET GUPTA SUBRAMANIAN S. IYER 24 SEP 2019*

IBM J. RES. & DEV. VOL. 63 NO. 6 PAPER 5 NOVEMBER/DECEMBER 2019

Objective: allow bare chips (chiplets or dielets) interconnections faster at larger dimensions by using Silicon as support rather than PCB- SoC System on Chip

- Chip-to-chip spacing 100um rather than 1mm
- Remove interposers
- Substitute bump-bonding with 2-10um copper pillars

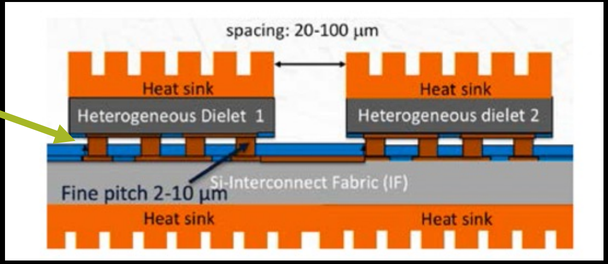

- Reduce wiring distances to 2um
- Use multiple layer wiring
- Reduce I/O ports distances to10 µm apart instead of 500 µm
- Chips support material and thermal matching

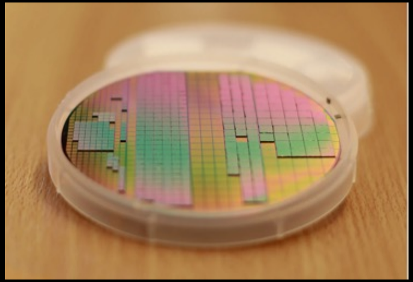

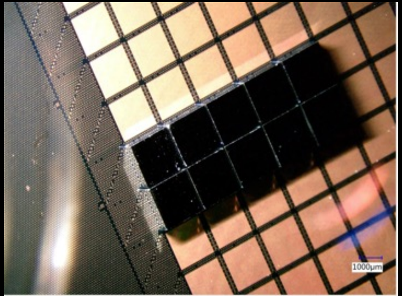

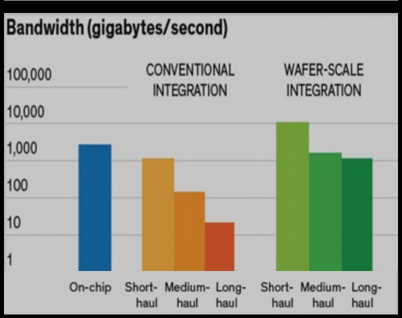

New generation of superfast chips with on wafer interconnectivity

IEEE Spectrum

SAMUEL K. MOORE 01 JAN 2020

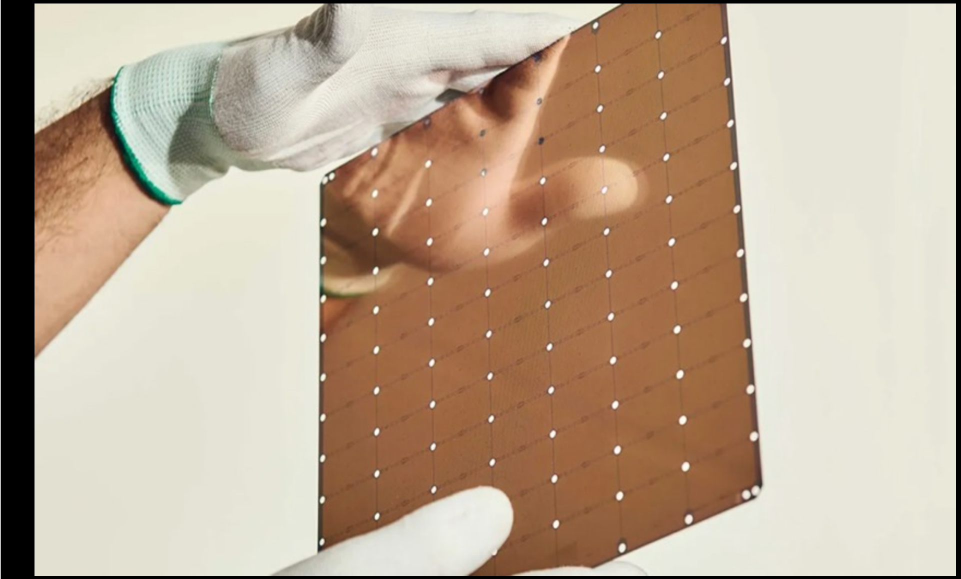

CEREBRA AI super-Computer

- The processing cores are not separated but interconnected directly at wafer level

- 46,255 square millimeters
- 1.2 trillion transistors,
- 400,000 processor cores,
- 18 gigabytes of SRAM
- interconnects capable of moving 100 million billion bits per second
- More than 10000 times faster than a GPU

- AI neural networks that previously took months to train can now train in minutes

- The Joule Supercomputer costs tens of millions of dollars to build, with 84,000 CPU cores spread over dozens of racks, and it consumes 450 kilowatts of power.

- Cerebras computer is 200 times faster, costs several million dollars and uses 20 kilowatts of power.

Precision in space and time Developments in Bulk Micro-Fabrication

Deep Reative Ion Etching

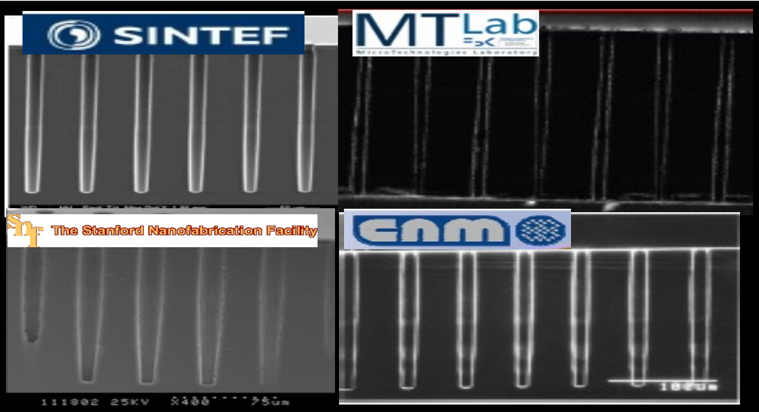

11:1
1997

24:1
today

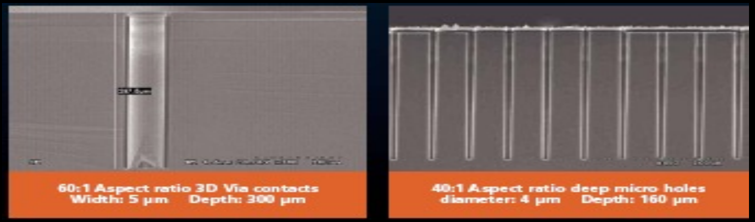
60:1 Aspect ratio 3D Via contacts
Width: 5 µm Depth: 300 µm

40:1 Aspect ratio deep micro holes
diameter: 4 µm Depth: 160 µm

40-60:1

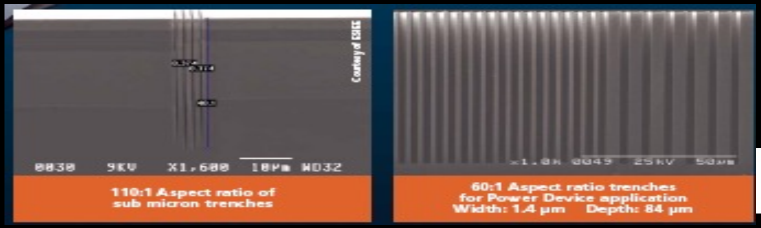

110:1 Aspect ratio of
sub micron trenches

60:1 Aspect ratio trenches
for Power Device application
Width: 1.4 µm Depth: 84 µm

110:1!!!

ALCATEL
Micro Machining Systems

Cryo-etching

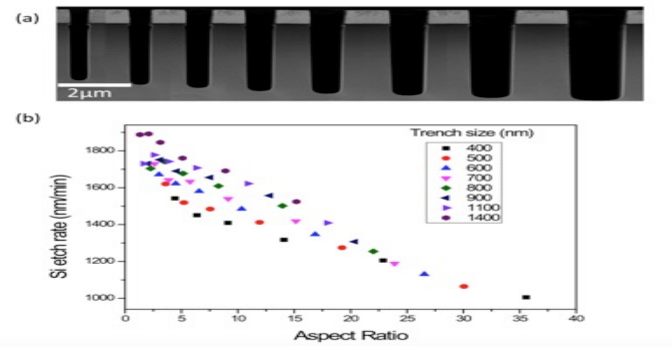

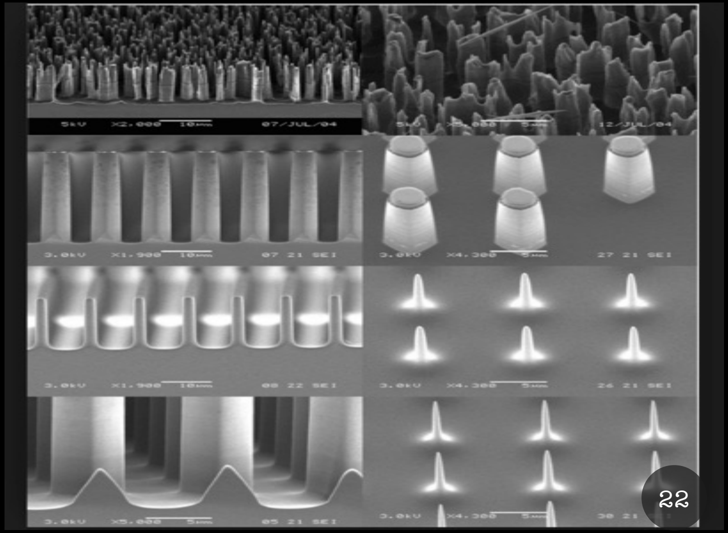

Voltage/Thermal Management

Micro-channel cooling Front. Phys., 22 April 2021[*https://doi.org/10.3389/fphy.2021.633970*](https://doi.org/10.3389/fphy.2021.633970)

BURIED INTERCONNECTS WILL HELP SAVE MOORE'S LAW , Brian Cline, Divya Prasad, Eric Beyne & Odysseas Zografos *IEEE Spectrum, September 2021*

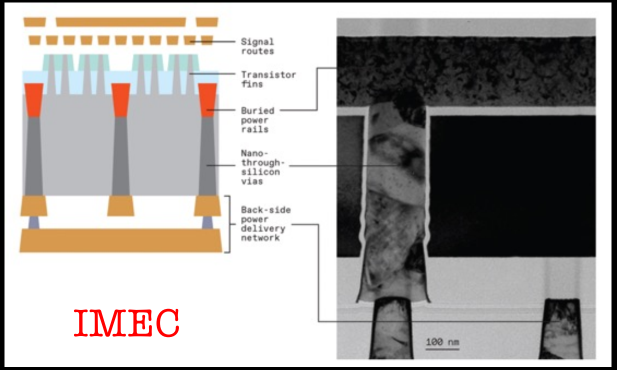

- Moving the power-delivery network to the other side of the silicon—the "back side"—reduces voltage loss because all the interconnects in the network can be made thicker to lower resistance.
- Removing the power-delivery network from above the silicon leaves more room for signal routes, leading to even smaller logic circuits and letting chipmakers squeeze more transistors into the same area of silicon.
- The removal of metal layers and connections also reduces power consumption.

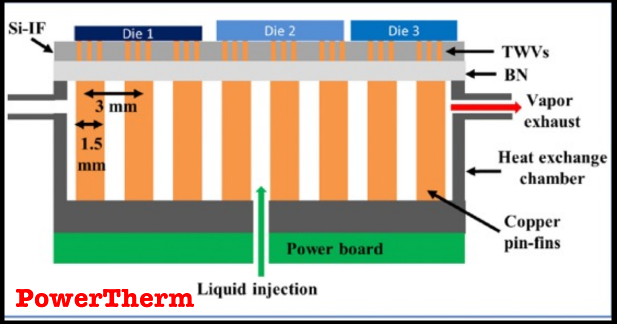

Proc. IEEE Intersoc. Conf. Thermal Thermomech. Phenomena Electron. Syst., May 2019, pp. 1228-1233

For a heterogeneous Si-F system, composed of :

- 4:1 ratio of memory (75%) and processor (25%) dielets, where each memory dielet dissipates 0.2 W/mm^2 and each processor dielet dissipates 0.5 W/mm^2, a 300-mm SoW is expected to dissipate up to 20 kW of power

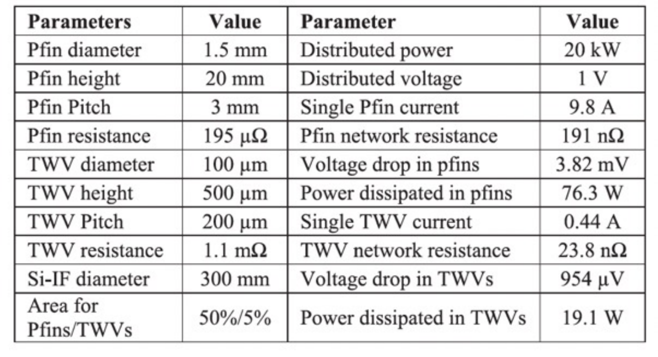

Parameters	Value	Parameter	Value
Pfin diameter	1.5 mm	Distributed power	20 kW
Pfin height	20 mm	Distributed voltage	1 V
Pfin Pitch	3 mm	Single Pfin current	9.8 A
Pfin resistance	195 μΩ	Pfin network resistance	191 nΩ
TWV diameter	100 μm	Voltage drop in pfins	3.82 mV
TWV height	500 μm	Power dissipated in pfins	76.3 W
TWV Pitch	200 μm	Single TWV current	0.44 A
TWV resistance	1.1 mΩ	TWV network resistance	23.8 nΩ
Si-IF diameter	300 mm	Voltage drop in TWVs	954 μV
Area for Pfins/TWVs	50%/5%	Power dissipated in TWVs	19.1 W

3D Detectors and applications

Radiation sensors with three-dimensional electrodes, CRC Press, Boca Raton, U.S.A., 2019

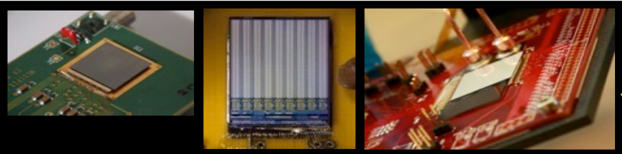

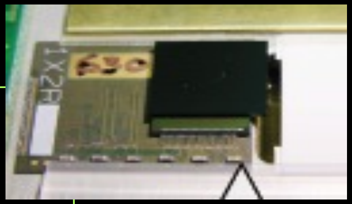

Extreme
Radiation
Hardness
20%@10^{17}ncm^{-2}

ATLAS FE-I3
ATLAS FE-I4 (with micro-channels)
AFP
Medipix/Timepix
CMS

LHC-Upgrades

Silicon +ASIC

Consolidated

Silicon +Converter

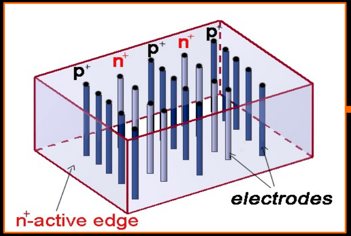

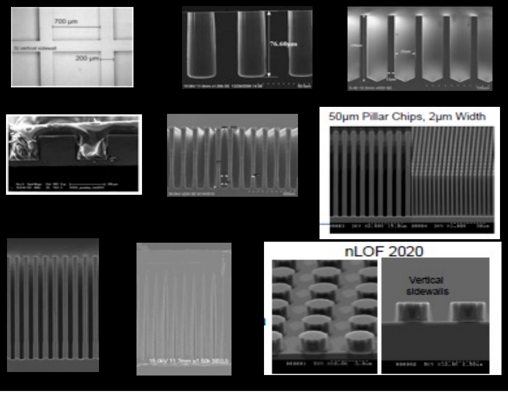

Neutron
Detectors

~50%
efficiency

- GaAs
- CdTe
- Diamond
- a-Si

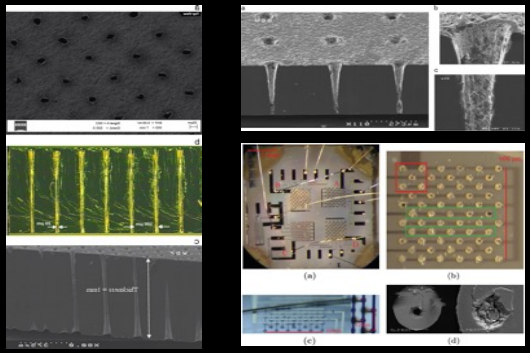

New Materials

Emerging

New Shapes

- Core shell
- Curved
- Edge
- Ring..

Unprecedented time
resolution
1ps with trench electrodes

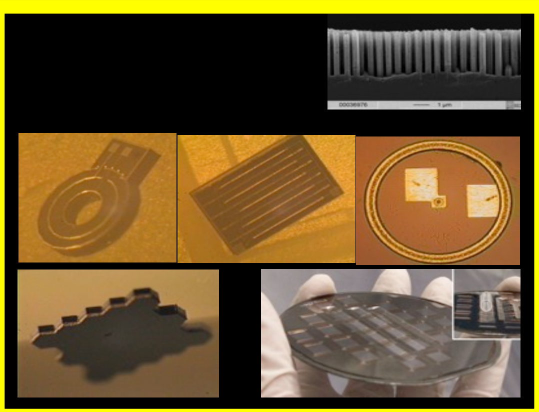

Conclusions

- Micro-fabrication
- 2D materials
- Meta-materials
- Nano-materials
- 3D printing
- Quantum Imaging

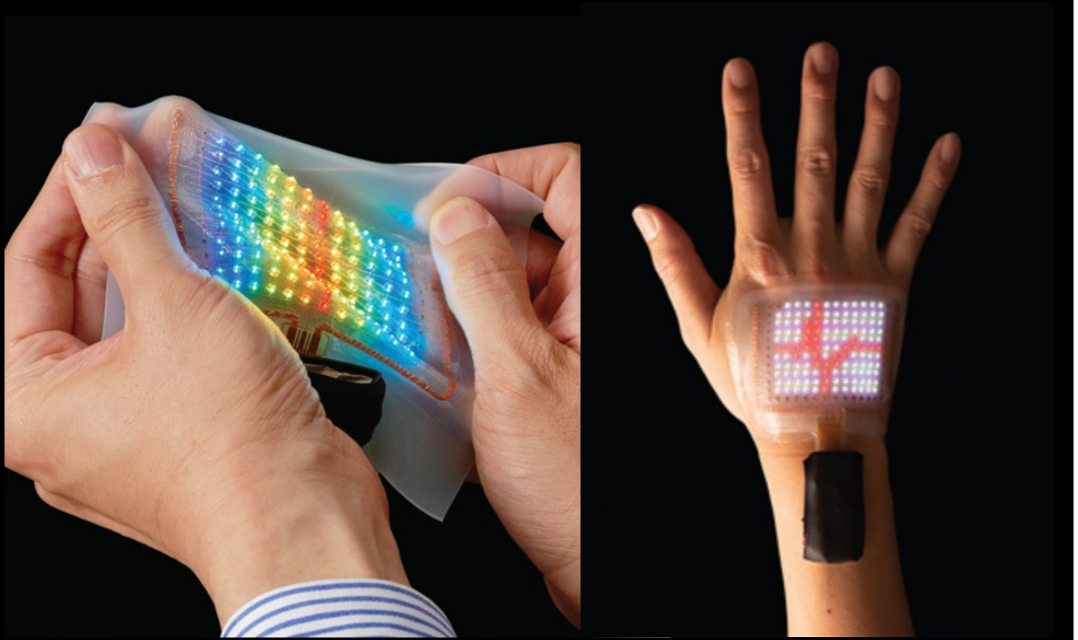

Stretchable, Bendable, Bodyconforming Electronics IEEE Spectrum June 2021

are the technologies to keep on the radar for solutions to precision detectors for the next generation of "imagers" in science and real life but it might take some time to get to the industrialization needed to produce the volume we need.
More emerging ones might also be coming available faster than we think.